ER Environmental Review Journal
Volume 11 No.2, 2026.
ISSN:1118-7190

ASSESSMENT OF SURFACE DAYTIME URBAN HEAT ISLAND DYNAMICS IN ONITSHA FROM 2010 – 2023.

[1*]Oruche, C., [1]Enete, I.C. and [1,2]Nzoiwu, P.C.
[1]Department of Geography and Meteorology, Nnamdi Azikiwe University, Awka, Nigeria
[2]Earth Systems Observation Lab, Nnamdi Azikiwe University, Awka, Nigeria.
Corresponding author: Email address: orasonicpeter@gmail.com

ABSTRACT
This study assessed the surface daytime urban heat island and land use/land cover change *dynamics in Onitsha from 2010 to 2023. The objectives of the study include the determination of land surface temperature, the magnitude of UHI, and measures to mitigate UHI in the study area. The research design adopted in this study is the survey design. Multitemporal Landsat ETM+ and OLI images were obtained at 7-year intervals for 2010, 2017, and 2024, respectively. The images obtained were classified using the supervised classification techniques. The result showed that LST varies from a range of 23.8 – 33.1 ºC in 2010, to 24.9 – 33.1 ºC in 2017, and 25.4 – 38.8 ºC in 2024. By 2024, extreme heat dominated much of the city, given a dramatic intensification of high LST values across Onitsha compared to 2010 and 2017. For the western part of the city, termed the coolest, the extent of this coolest range has further contracted compared to 2017 (21.8–24.8°C) and 2010 (21.4–23.7°C), with more areas near the river shifting into the 25.4–28.7°C range, indicating continued warming even in this thermally modified zone. The determined UHI magnitude revealed a UHI magnitude of 1.9°C in 2010, which increased to 2.4°C in 2017 and further grew to 2.6°C by 2024 though ANOVA revealed that the observed variations in LST across the years are not statistically significantly different. The progressive increase highlights the intensification of the UHI effect in Onitsha, driven by rapid urbanization, population growth, and land use changes. The study recommends the setting up of afforestation programs to intentionally modify the microclimate of the Onitsha urban area, check urban sprawl, and ensure continuous monitoring using remote sensing techniques.*

1. Introduction

The land environment is an important natural resource on which most activities are based. The uses to which the land is subjected to, is continuously changing, resulting to variations in its biophysical characteristics. The biophysical characteristics of the earth's surface refers to its land cover while the modifications in cover characteristics of the land environment currently experienced globally has been attributed to uses to which humans subject land (Nzoiwu, Ozoemene and Emelugini, 2020). The land use at any particular time represents the cumulative effects of a myriad of decisions and actions by humans. These activities combine to alter the geometry of the earth's surface. Urbanization is a key human-induced activity driving change in land uses and land cover. This is further intensified by growing global population, with over 54% of the global population being urban dwellers (Ayanlade, 2016), which has been predicted to increase to 68% by 2050 (United Nations, 2019; Li and Zhang, 2021). Thus, as global population rises, there is increasing demand on the available land for more settlements, roads, shelter and changes in lifestyle which has invariably led to the increased encroachment on natural vegetation.

Continued encroachment on natural vegetation and transitioning to other types of land use such as urban lands is known to modify the biophysical and biogeochemical properties associated with surface energy processes. Land-use changes due to urbanization cause a wide range of environmental impacts within the urban and semiurban environments. One such impact is the urban heat island (UHI) phenomenon. This phenomenon is a consequence of inadvertent climate modifications resulting in elevation of near-surface air temperatures due to surface vegetal removal peculiar to urbanization. Zargari, Mofidi, Entezar and Baaghideh (2024) described urban heat island as a microclimatic phenomenon that occurs in urban environments, in which urban air temperatures are higher than rural air temperatures. The phenomenon is expected to continue to increase and worsen as more people are expected to reside in urban areas by 2050 based on the UN report released in 2019. Therefore, more heat-absorbing surfaces such as built areas are expected to replace more natural land cover and more people are now expected to be exposed to temperature and heat stress (Zhang et al., 2022). Thus, the effects emanating from UHI has become a major health concern for urban residents such as urban heat stress and the associated mortality rates (Zhou, 2017).

Following the increasing environmental and health awareness of the potential effects of UHI and its intensity, efforts have been underway to explore reliable methods to evaluate the impact of UHI. These scientific interests range from studies that attributes UHI intensity to urban-rural contrast of aerodynamic resistance followed by change in evaporation efficiency (Zhao et al., 2014), to studies that shows that the variations in daytime UHI intensity is due to urban-rural contrast in evaporation capacity related to surface resistance (D Li et al., 2019). There are other studies that applied prediction models such as urban canopy models to understand surface UHIs (Broadbent et al., 2018; Moradi et al., 2022). Advances in GIS and remote sensing have enables numerous researches to employ satellite imageries like MODIS Aqua, Sentinel and Landsat to monitor and evaluate UHI (Jumari et al., 2023). These researches relied on land surface temperatures (LST) derived from remotely sensed imageries to study the contributions of land use and land cover dynamics to SUHI occurrence (Adinna, Enete and Okolie, 2019; Choi, Suh and Park, 2014; Abuloye et al., 2015; Nzoiwu et al, 2017; Yang, Huang and Li, 2017). Studies have also sought to establish the possible drivers of urban heat island using urban ecohydrological models (Zhang et al., 2022). Some have linked this phenomenon as the outcome of surface modifications in urban environments were vegetations are replaced by synthetic surfaces, which increases ambient temperature beyond what is obtainable in nearby countryside. Others like Ayanlade et al. (2016) have also linked this phenomenon as the outcome of huge amount of heat generated from industrial activities and other anthropogenic heat sources in an urban area.

However, as people and structures increasingly become concentrated in urban areas like Onitsha, with reduction in vegetal cover, urban heat island effects will exacerbate – an elevated temperature of urban areas relative to rural surroundings (Oke, 1973). This makes urban areas and their dwellers more vulnerable. Elevated temperatures due to UHI effect increases energy consumption such as in air conditioning in cities and causes the release of additional air pollutants in the course of more energy generation. This further degrades the quality of air in urban environments as more greenhouse gases get emitted, affecting the drive towards achieving sustainable cities. Hence, given the global pursuit for climate change mitigation and adaptation, the understanding of the UHI aspect of urban climatology becomes pertinent, knowing that such knowledge would help shape Onitsha into a more climate-resilient, sustainable and livable city.

2. Materials and Methods

2.1 Study Area

Onitsha is located between longitudes 6^0 45^1E and 6^0 50^1 E, and latitudes 6^0 6^1 N and 6^0 10^1 N. The Onitsha urban area is made up of two local governments authorities (LGAs) in Anambra State – Onitsha North and South LGAs. The western border of the city is bound by River Niger and Delta State, to the south by Ogbaru LGA, to the east by Idemili North LGA, while Oyi LGA is in the northeast border, and Anambra East and West LGAs to the north (Figure 1).

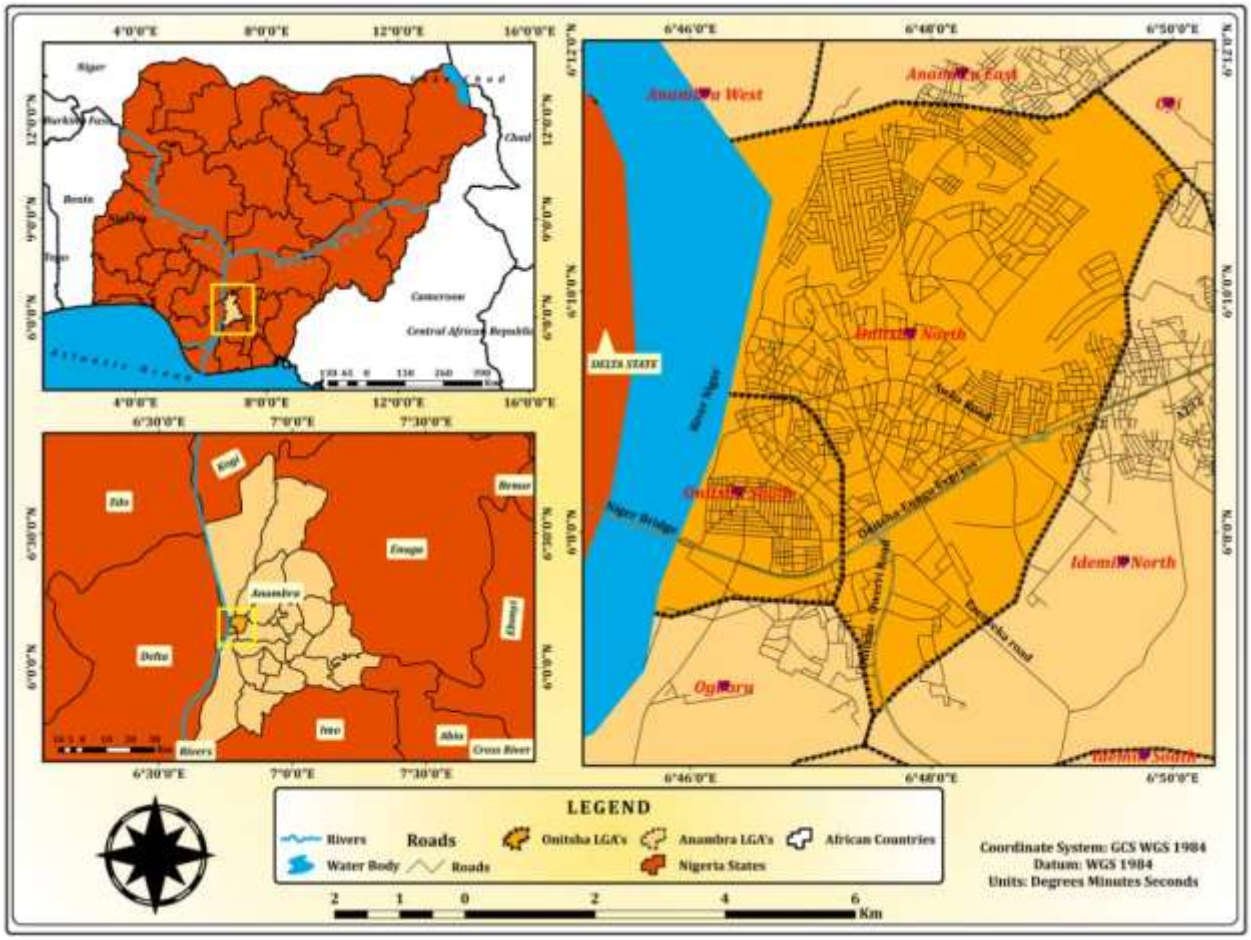


Fig 1: Map of Onitsha (Source: GIS Lab, Dept. of Geography and Meteorology, N.A.U)

The main geological feature of the urban area is the Bende – Ameki formation which has its lateral facies equivalent to the Nanka formation (Okoye, Ezenwaji, Nzoiwu and Igboanugo, 2024). In terms of topography, the study area has generally a gentle topography, that slopes from Army barracks in the east to the river Niger in the west, with uplands around Trans-Nkisi and 3-3 areas and Awada district.

Onitsha is located in the transition zone between the tropical Monsoon climate and the tropical savanna climate. There are two main seasons – the wet and the dry seasons. It has a mean annual rainfall of 1817mm (Ezenwaji, 2018). Rainfall usually starts in early March and ends in

November indicating a rainfall duration of eight months, while the remaining four months constitutes the dry season. The temperature of Onitsha averages between 23℃ *and* 27℃ with the month of March experiencing the hottest weather. Relative Humidity is equally high ranging from 70 percent to 80 percent with the highest value being recorded between June and October, which is during the heart of the rainy season. Onitsha lies on the Niger-Anambra floodplain basically within the Nkisi and Idemili rivers watersheds of the lower River Niger basin. There are three main rivers in Onitsha: the river Niger, the Idemili River and the Nkisi River. The river Niger is the largest of the rivers in terms of size and discharge, followed by the Idemili river which rises from Awka upland around Anaocha LGA and empties into the river Niger at Onitsha. Also, the Nkisi river drains the old Akpaka forest reserve in the northern parts of the town. The population of Onitsha according to the 2006 Census figure is 256,941 but Anambra State government has questioned the veracity of the figure reasoning that it is grossly underrepresented stating that the 2022 population of town should be above 1,000,000 (Anambra State Government, 2022). However, our projection of the population of the urban area, as well as, the already engulfed neighbouring LGAs, using the 2006 figure as the base, as well as, parts of other neighbouring LGAs is 1,188,166 (Okoye et al., 2024). Onitsha covers a total land area of 68.72sqkms of which about 42.90sqkm or 62 percent of the land are completely built up.

2.2 Data collection and pre-processing of imageries

The LANDSAT data was downloaded from USGS Earth Explorer. The Enhanced Thematic Mapper plus (ETM+) image was obtained for 2010 and 2014. The Operational Land Imager (OLI) for 2018 and 2023. The researcher deliberately chose the intervals of 4 years to ensure uniformity between the datasets. The Landsat satellite data have a 30m spatial resolution, and the ETM+ images have a spectral range of 0.45-2.35 micrometers (μm), with bands 1 to 7 and 8, respectively. Meanwhile, the Operational Land Imager (OLI) extends to band 12. They were used for image classification and LST extraction. Monthly Land Surface Temperature (LST) data at a spatial resolution of 1000m was obtained from EOS-Terra-MODIS L3 composite products (MOD11C1). The LST data includes daytime (~13:30) and night-time (~23:30) temperature observations for Jan 2013 through to December 2023. MODIS has a high temporal resolution (0600 hrs), making it ideal for temporal trend assessment. The administrative map of Nigeria containing states and LGAs was obtained from the National Space Research and Development Agency (NASRDA). It is a projected vector shapefile that was used to specify the boundary of the study area. Table 1 gives a detailed description of the datasets used.

Table 1: Data used and their sources with brief description of characteristics

S/N	DATA	SENSOR	BAND	SPATIAL (TEMPORAL) RESOLUTION	SOURCE	DATE	REFERENCE SYSTEM
1	LANDSAT 7	ETM+	2-5	30m (16Days)	USGS Earth Explorer (Online)	2010	WGS 1984 UTM ZONE 32N
			6 (Thermal)	30m (16Days)		2014	
2	LANDSAT 8	OLI	3-6	30m (16Days)	USGS Earth Explorer (Online)	2018	WGS 1984 UTM ZONE 32N
		TIR	10-11 (Thermal)	30m (16Days)		2023	

3	MODIS	TERRA	31-32	1000m (6 Hours)	EARTHDATA/ NASA-EOS	2001-2023	WGS 1984 UTM ZONE 32N
4	Administrative and LGA Map of Nigeria				NASRDA	2015	WGS 1984 UTM ZONE 32N

The Landsat data, were captured under clear conditions (0% cloud coverage for all the images), were used, hence uniform atmospheric conditions within the images was assumed and no atmospheric corrections may need to be applied. All the images were pre-processed by the USGS to rectify any geometric or radiometric distortions of the image. This correction process employs both Digital Elevation Models (DEMs) and Ground Control Points (GCPs) to achieve a product that is free from distortions related to the Earth (e.g. curvature, rotation), satellite (e.g. attitude deviations from nominal), and sensor (e.g. view angle effects). The USGS also geometrically corrected and georeferenced both images to the WGS1984 datum and Universal Transverse Mercator (UTM) zone 32N coordinate system.

For the Landsat ETM+ and OLI, a False Colour Composite (FCC) operation was performed using the ArcGIS 10.4 software and the images were combined in the order of band 5, 4 and 3 for Landsat ETM+ while that of Landsat OLI was in the order of band 6, 5 and 3 due to change in sensor. The images were clipped to the boundary of Onitsha to allow for more detail and accuracy. A supervised classification scheme with the interactive selection algorithm was used for the classification. The supervised classification was performed by creating a training sample, and based on spectral signature curve, various land-use classes were created. These classes were observed individually on the clipped image and was used for the classification. Table 2 shows the characteristics of these classes and the colours that were assigned to them.

Table 1. Land Use/Land Cover classes and descriptions (Source: Andualem et al., 2018; Nzoiwu et al., 2020)

Class	**Land Use**	**Description**	**Examples**	**Observed Colour**	**Assigned Colour**
1	Water Body	Surface water bodies	River, permanent open water, lakes, ponds, canals, permanent/seasonal wetlands, low-lying areas, marshy land, and swamps.	Navy Blue	Lapis Lazuli
2	Built Up	Impervious surfaces that do not allow infiltration of water	All infrastructure—residential, commercial, mixed use and industrial areas, villages, settlements, road network, pavements, and man-made structures.	Cyan blue, Purple, white	Poinsettia Red
3	Bare Surface	Includes all open grounds that are neither vegetated nor built-up,	Fallow land, earth and sand land in-fillings, construction sites, developed land, excavation sites, open space, bare soils, and the remaining land cover types.	Light and dark brown, cream.	Topaz Sand

		untarred roads and footpaths.			
4	Vegetation	This includes all plants along river channels, forests, parks and reserves, farmland etc.	Trees, natural vegetation, mixed forest, gardens, parks and playgrounds, grassland, vegetated lands, agricultural lands, and crop fields.	Light, lemon and dark green	Quetzel Green

2.3 Retrieval of Land Surface Temperature (LST) from Landsat Images

The mono-window algorithm method was adopted to retrieve the LST from the imageries selected for this study. The Landsat ETM+ band 6L (10.4 – 12.5 µm) and TIRS 10 and 11 (10.60 -11.19 µm) have a spatial resolution of 30m respectively which is considered suitable as shown by many literatures for capturing the multifaceted intra-urban temperature differences thus making it effective for urban climate analysis. For the Landsat ETM+ sensor, images in the thermal band are taken twice: one in the low-gain mode (band 6L) and the other in the high-gain mode (band 6H). Band 6L is used to image surfaces with high brightness, whereas band 6H is for low brightness. Band 6L was used in this study, due to errors contained in the 6H band. Consequently, the Landsat thermal bands were used to retrieve LST over the study area for the four different periods (2013, 2017, 2020, and 2023) based on the following steps:

Step 1. Conversion of Digital Numbers (DN) of the bands to Spectral Radiance

The DN of the thermal bands ETM+ were converted into spectral radiance values for each of the investigated years using the following equation –

$$L_\lambda = \left(\frac{L_{MAX} - L_{MIN}}{Q_{CALMAX} - Q_{CALMIN}}\right) \times (DN - 1) + L_{MIN} \quad _ \quad _ \quad _ \quad (1)$$

Where;

L_λ = The spectral radiance at the sensor's aperture in $Wm^{-2}\ sr^{-1}\ \mu m^{-1}$

L_{MAX} = Spectral radiance scaled to Q_{CALMAX} in $Wm^{-2}\ sr^{-1}\ \mu m^{-1}$, available in the metadata.

L_{MIN} = Spectral radiance scaled to Q_{CALMIN} in $Wm^{-2}\ sr^{-1}\ \mu m^{-1}$, available in the metadata.

Q_{CALMAX} = Maximum quantized calibrated pixel value (corresponding to L_{MAX}) in DN = 255

Q_{CALMIN} = Minimum quantized calibrated pixel value (corresponding to L_{MIN}) in DN = 1

DN = Digital Number of the Band

For Landsat 8 with file data on Radiance Multiplier (M) and Radiance Add (B), the thermal infrared (TIR) band were converted into spectral radiance (Lλ) using the equation -

$$L\lambda = M_L Q_{CAL} + A_L \quad _ \quad _ \quad _ \quad _ \quad _ \quad _ \quad (2)$$

Where;

L_λ = The spectral radiance at the sensor's aperture in Wm^{-2} sr^{-1} μm^{-1}

M_L = Band Specific Multiplicative Rescaling factor, gotten from the metadata of the image

Q_{CAL} = Quantized & calibrated standard product pixel values (Digital Number)

A_L = Band Specific Additive Rescaling factor, gotten from the metadata of the image.

STEP 2. Conversion from Spectral Radiance to At-Satellite Brightness Temperature

Spectral radiance values for the bands will then be converted to radiant surface temperature under an assumption of uniform emissivity using pre-launch calibration constants for the Landsat ETM+ sensor implemented into this equation;

$$T = \frac{K_2}{ln\left(\frac{K_1}{L_\lambda}+1\right)} - 273.15 \quad _ \quad _ \quad _ \quad _ \quad _ \quad _ \quad (3)$$

Where;

T = At-satellite brightness temperature in Degrees Celsius

L_l = Spectral radiance in Wm^{-2} sr^{-1} μm^{-1} (gotten from equations 4 and 5)

K_1 = Band specific thermal conversion constant from the metadata (K1_CONSTANT_BAND_X, x is the thermal band number)

K_2 = Band specific thermal conversion constant from the metadata (K2_CONSTANT_BAND_X, x is the thermal band number)

-273.15 = Constant for conversion from Kelvin to Degrees Celsius

STEP 3. Correcting for Land Surface Emissivity (LSE)

In estimating LSE, Normalized Differential Vegetative Index (NDVI) were utilized for emissivity correction. The temperature values obtained using Equation (6) were referenced to a blackbody. Therefore, corrections for spectral emissivity (ε) became necessary according to the nature of land cover. This equation was used:

$$e = 0.004P_v + 0.986 \quad _ \quad _ \quad _ \quad _ \quad _ \quad _ \quad (4)$$

where, e = Land Surface Emissivity; 0.004 and 0.986 = Constants for emissivity estimation; P_V = Proportion of vegetation given by the equation –

$$P_V = \left(\frac{NDVI - NDVI_{min}}{NDVI_{max} - NDVI_{min}}\right)^2 \quad (5)$$

NDVI = Normalized Differential Vegetation Index as computed with Equation (1) for each of the years

$NDVI_{min}$ = Minimum value of NDVI for that year

$NDVI_{max}$ = Maximum value of NDVI for that year.

STEP 4. Estimation of the Land Surface Temperature

Finally, having corrected the emissivity in equation (7), the LST were estimated using the equation:

$$LST = \frac{B_T}{1+w} \times \frac{B_T}{P} \times \ln(\mathcal{E}) \quad (6)$$

where, LST= Land Surface Temperature in Degrees Celsius; B_T = At-satellite brightness temperature; W = Wavelength of emitted radiance (μm)

$$p = h \times \frac{c}{s}\ (1.438 \times 10^{-2} m\ K) = 14380 \quad (7)$$

h = Planck's constant ($6.626 \times 10^{-34} Js$)

S = Boltzmann constant ($1.38 \times 10^{-23} J/K$)

C = Velocity of light ($2.998 \times 10^{8} m/s$)

e = LSE

2.3.1 Extraction of LST from MODIS

MODIS is a polar-orbiting Earth Observing Satellite instrument that serves as the keystone for global studies of atmosphere, land and ocean processes. MODIS LST products have a temporal resolution of 0600hrs. It scans from nadir in 36 bands, with bands 1-19 and band 26 in the visible and near infrared range, and the remaining bands in the thermal infrared from 3-15 ±55 μm. The 36-band MODIS satellite scanner has 1 km^2 pixels at nadir for the thermal infrared bands that will be used for LST. The proposed algorithm employs the radiance and emissivity in band 31 and band 32. With 15 emissive bands, the Moderate Resolution Imaging Spectroradiometer (MODIS) on-board the EOS-TERRA platform offers new perspective in earth observation in the infrared

spectrum (3-15 µm). The LST products have already been processed, converted to brightness temperature and corrected for emissivity. However, a rescaling factor will be needed to extract the temperature values in degree Celsius. This is given as;

$$LST = DN \times 0.002 \quad (8)$$

where, LST = Land surface temperature in degrees Celsius; DN = Dataset in Kelvin; 0.002 = Rescaling factor.

This will be done for the day and night variables of each month.

2.3.2 Urban Heat Island Assessment

Points representing ten rural and ten urban areas in Onitsha will be generated and the urban heat island will be assessed using the equation;

$$UHI = T_U - T_R \quad (9)$$

where, UHI = Urban Heat Intensity; T_U = Temperature at urban station; and T_R = Temperature at rural station.

2.4 Statistical Analysis

Regression analyses and analysis of variance test were carried out to determine the relationship between land use/land cover and land surface temperature, and to determine whether the observed variations in LST values within the study period differ significantly. Also, the Students 't' Test is carried out to determine the significance of the difference between the urban and rural temperature values. The t-test was used to determine if two sets of data are significantly different from each other. The independent unpaired samples t-test was implemented due to the independent and identically distributed samples of the rural and urban temperature values. The t statistic to test whether the means are significantly different can be calculated as follows:

$$\boldsymbol{t} = \frac{\bar{X}_1 - \bar{X}_2}{\sqrt{\frac{(\delta 1)^2 + (\delta 2)^2}{n}}} \quad (10)$$

where, $\boldsymbol{\delta}_1$ and $\boldsymbol{\delta}_2$ = Standard deviation for N, N= Number of observations, $\bar{X}_1 - \bar{X}_2$ = Standard error of the difference between the two means. For significance testing, the degree of freedom for this test is given by: $N_1 + N_2 - 2$. where N= number of observations in each group.

3. Results and Discussion

This study assessed the spatiotemporal variation of Land Surface Temperature (LST) and Land Use and Land Cover (LULC) across Onitsha between 2010 and 2024. The findings reveal distinct trends in temperature and land cover changes and their interrelationships, and highlight the presence and intensification of the Urban Heat Island (UHI) effect in the area. Regarding spatiotemporal LST variation, the study observed different thermal environments across three periods: 2010, 2017, and 2024. In 2010, the maximum LST was 33.1°C, the mean was 29°C, and the minimum was 21.4°C, resulting in a range of 11.7°C (Figure 2).

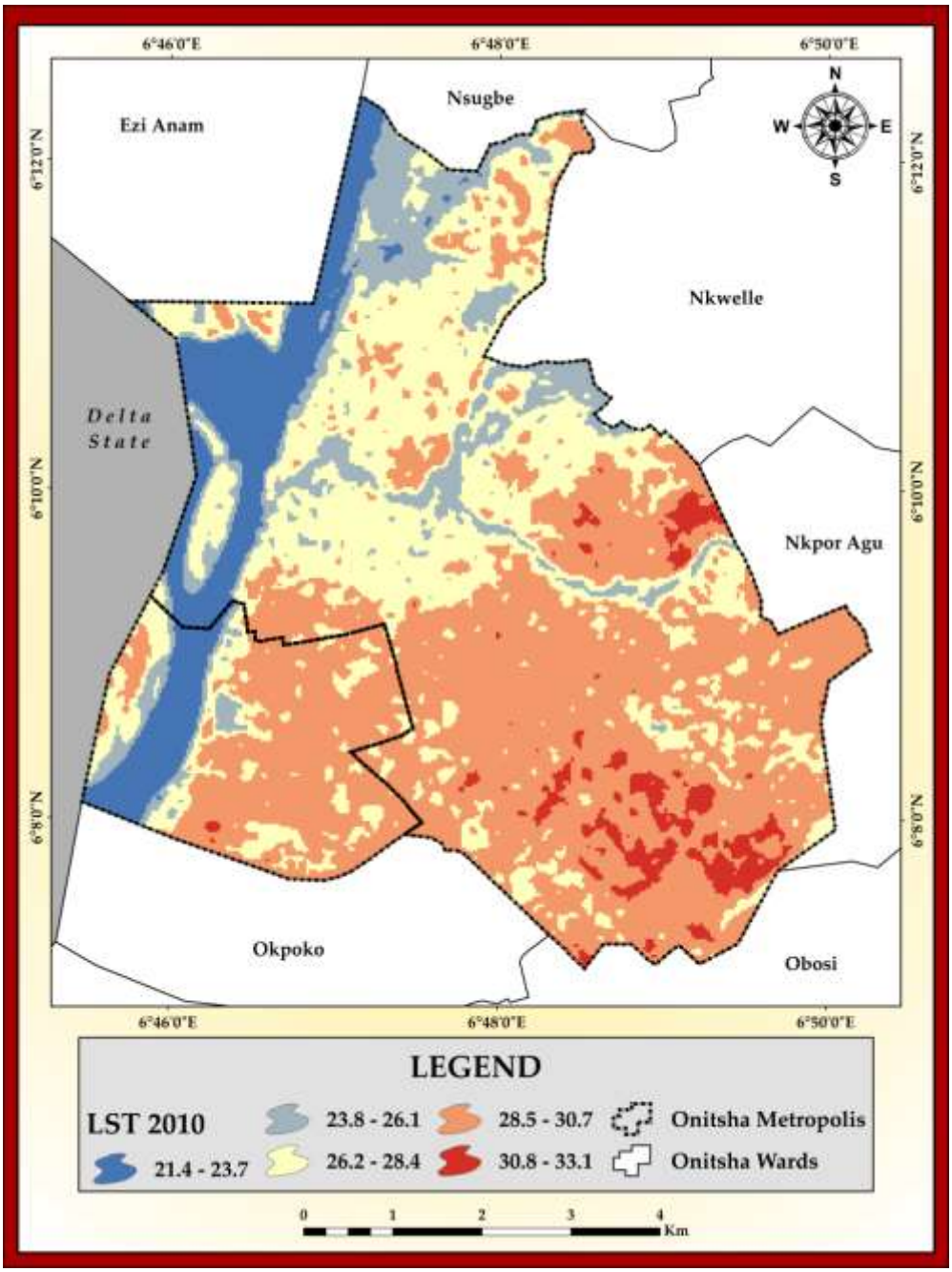


Fig 2: Onitsha LST Map for 2010

By 2017, the maximum remained 33.1°C, the mean slightly decreased to 28.9°C, and the minimum marginally increased to 21.8°C, narrowing the range to 11.3°C (Figure 3). This period suggested a relatively stable thermal environment with a slight cooling in the mean temperature. However, a significant shift occurred from 2017 to 2024, with the maximum LST rising sharply to 38.8°C, the mean increasing to 31°C, and the minimum edging up to 22°C, resulting in a wider temperature range of 16.8°C in 2024 (Figure 4). This marked increase indicates a pronounced warming trend, driven by factors

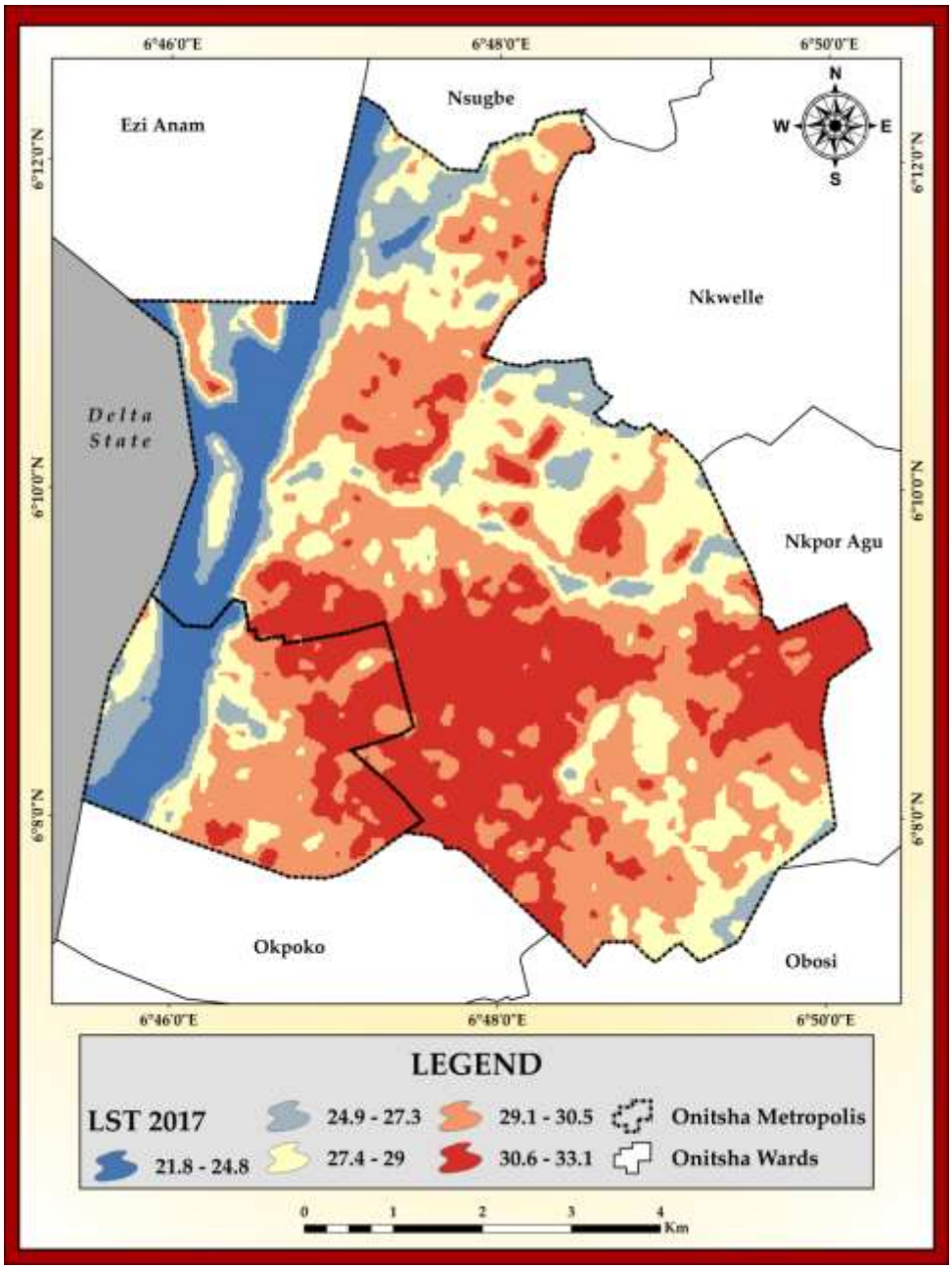


Fig 3: Onitsha LST Map for 2017

such as urbanization, population growth, and land cover changes associated with the expansion of impervious surfaces, which contribute to the UHI effect. A similar increase in the UHI trend has been reported in Sahoo et al (2022), who reported that UHI intensities increased steadily between 2000 and 2020 in their study area. Also, Choudhury et al (2023) acknowledged that the environmental implications of unchecked urban growth are rising temperatures and the intensification of UHI effects. In agreement with the findings of this study, Choudhury et al (2023) found that considerable growth in urban built-up and a reduction in cultivated land contributed to a progressive rise in LST in the Kamrup metropolitan district of India following their application of a machine learning algorithm.

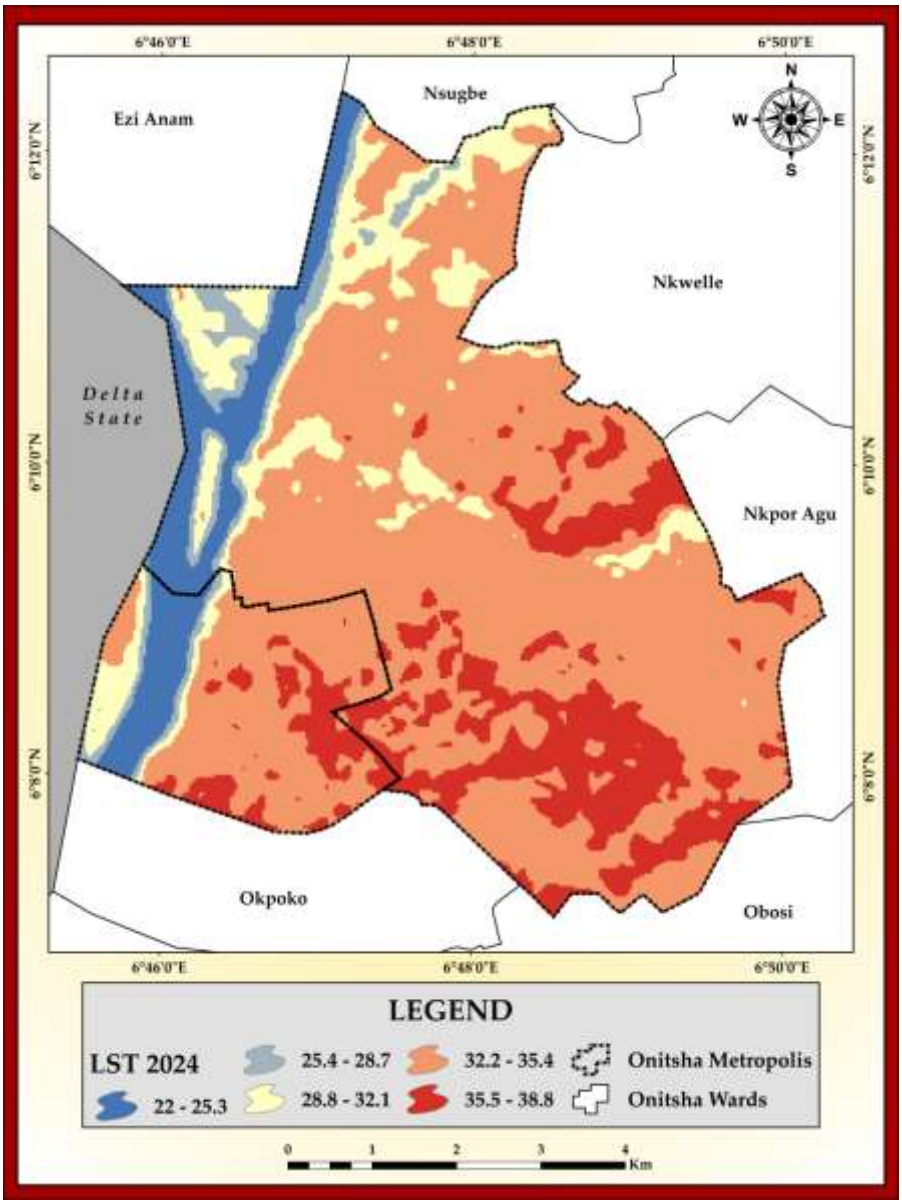


Fig 4: Onitsha LST Map for 2024

Furthermore, the western part of Onitsha, the Niger River area, consistently exhibited the lowest LST values across all years, predominantly ranging from 21.4–23.7°C in 2010, 21.8–24.8°C in 2017, and 22–25.3°C in 2024. This cooling effect is attributed to the presence of the Niger River, a natural heat sink through evaporative cooling and the higher thermal inertia of water bodies, as well as potentially more vegetation or less impervious surface cover near the river. Tiwari and Kanchan (2024) highlighted through their findings that water bodies and a healthy vegetation cover are necessary to maintain the LST and its related problems in Varanasi city, Uttar Pradesh region of India. However, the extent of this coolest range contracted over time, indicating warming even in this moderated zone. In contrast, the central and eastern parts displayed higher LST values. By 2010, warmer zones were mainly 28.5–30.7°C and 30.8–33.1°C, corresponding to densely built-up areas and contributing to the UHI effect. The highest LSTs were concentrated in the southeastern region near Obosi and parts of Okpoko. By 2017, the hottest category (30.6–33.1°C) had expanded westward into the central-southern region. The 2024 map showed a dramatic intensification of high LSTs, with the 35.5–38.8°C range becoming widespread across the central-southern (near Okpoko), southeastern (near Obosi), and eastern areas (near Nkpor Agu). The 32.2–35.4°C range was also extensive. This increasing trend from 2010 to 2024 depicts a substantial thermal shift driven by urban expansion and regional warming. The Urban Heat Island (UHI) Magnitude in Onitsha was determined by comparing the average temperature difference between urban and surrounding rural areas. The urban areas consistently showed higher temperatures than rural areas, indicating the presence of a UHI effect (Figures 5 and 6).

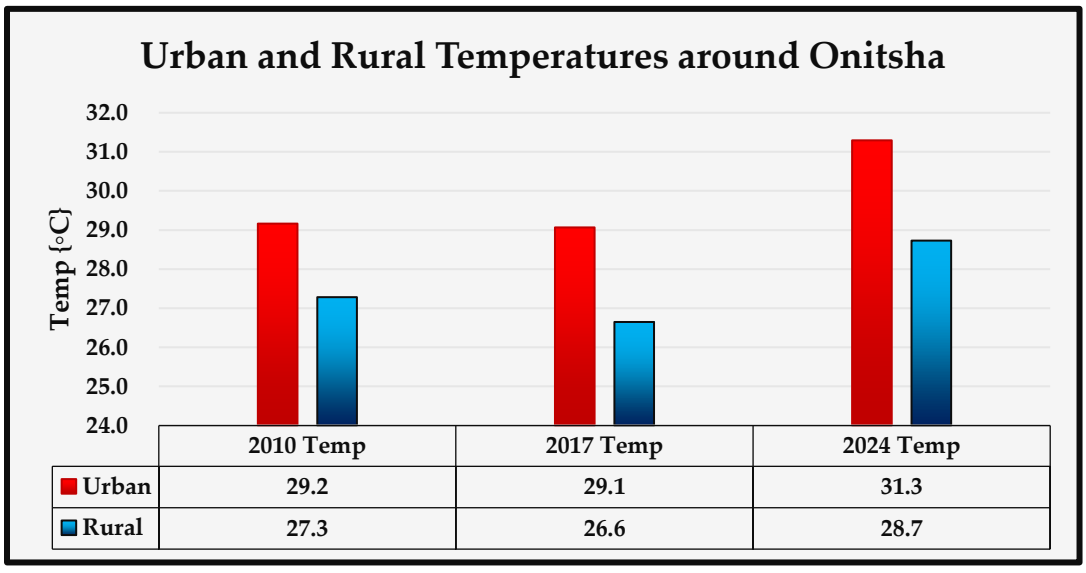


Fig 5: Urban and Rural Temperatures at Onitsha Metropolis

In 2010, the urban average temperature was 29.2°C, and the rural average was 27.3°C, resulting in a UHI magnitude (ΔUrban-Rural) of 1.9°C. By 2017, urban temperature was 29.1°C and rural

was 26.6°C, increasing the UHI magnitude to 2.4°C. By 2024, urban temperature rose significantly to 31.3°C, and rural to 28.7°C, further growing the UHI magnitude to 2.6°C. This progressive increase highlights the intensifying UHI effect in Onitsha, likely driven by rapid urbanization and land use changes, specifically the expansion of Built-up Areas. The intensity of the temperature in the comparatively smaller urban area is further depicted when considering the total area of urban (80.2 sq.km) versus rural areas (262.1 sq.km). Consequently, several mitigation measures are proposed, informed by the study's findings.

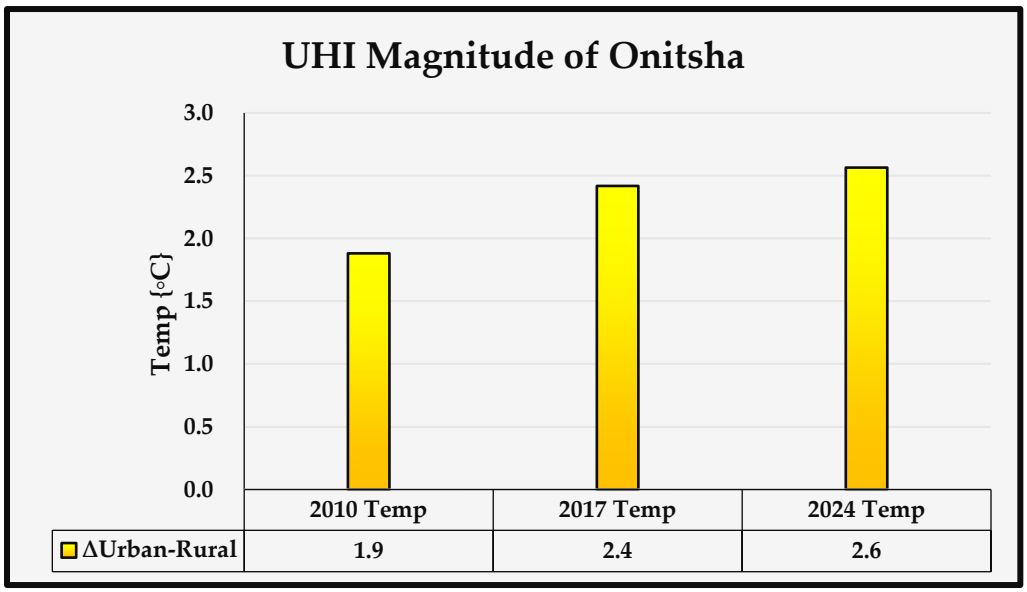


Fig 6: Chart of UHI in Onitsha

Furthermore, the correlation analysis was used to determine the relationship between the rate of change in LULC classes over time and the change in LST. A similar application of Pearson's correlation method was used in Tiwari and Kanchan (2024). This result showed a correlation coefficient (r) of 0.7 and a coefficient of determination (r^2) of 0.49 (Figure 7). The positive slope

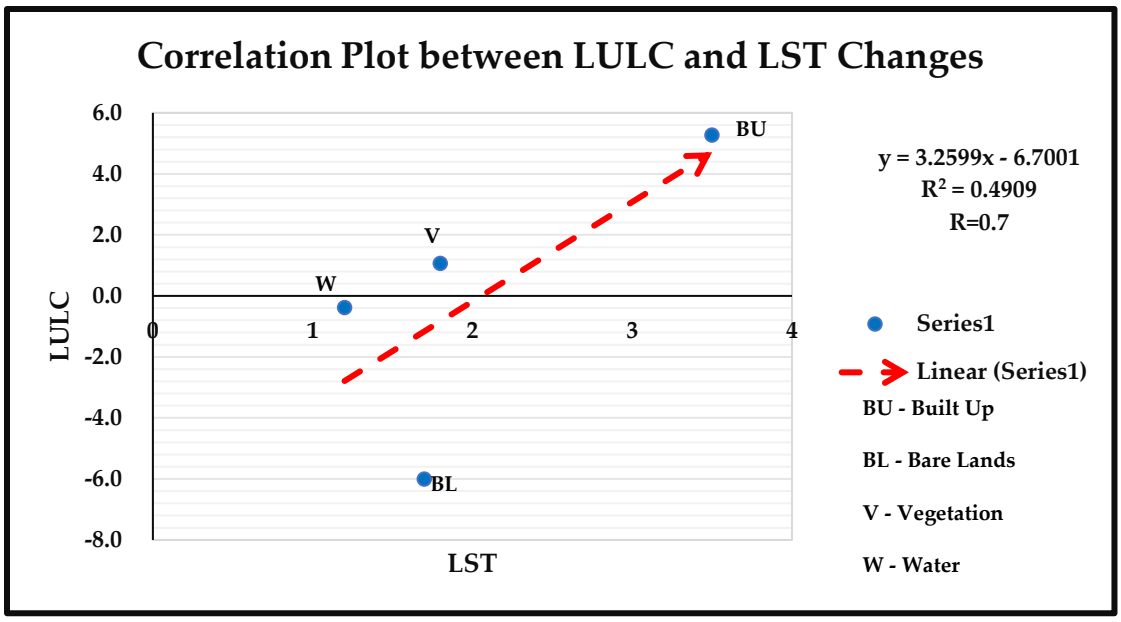


Fig 7: Correlation Plot between LULC and LST

of the trend line (3.2599) shows that as LST increases, LULC change tends to increase, with Built-up Area (LST 3.5, LULC 5.3) showing the highest values, reflecting urban expansion. Conversely, Bare Lands (LST 1.7, LULC -6.0) and Water (LST 1.2, LULC -0.4) show negative or minimal LULC changes, indicating potential reduction or stability. The correlation coefficient values indicate the presence of a strong positive relationship, indicating that higher LST changes are associated with higher LULC changes in the study area. However, to test the significance of this relationship, the t-test was used. This reveals that at a 95% level of confidence ($\alpha = 0.05$), the t-calculated of 1.386 is less than the critical t-table value of 4.303. Hence, while a positive relationship exists between LST and LULC changes in Onitsha Metropolis, this is considered not strong enough.

Table 3 shows the variation between the group results and the variation within each group. The F statistic simply shows the ratio between groups/within-group variability, or the ratio between the variance estimates. From the table 2, it can be deduced that the $F(2, 9) = 0.301$, $p = 0.746$ simply shows that the ratio between group/within group is approximately 4 times. Therefore, such a very low F statistic depicts that H_o cannot be rejected, given a high p-value, and one can easily conclude that the difference between group of LST values over time in the study area is much less than the group noise. Therefore, the result showed that the observed difference in the LST changes is statistically not significant, given a p-value of 0.746, which is greater than the alpha value of 0.05. This confirms the position of the F statistic. This outcome differs from the findings of Jumari et al (2023), who reported that their ANOVA test substantially showed that observed surface temperature changes were significant.

Table 3: ANOVA

Source of variation	Sum of squares	df	Mean square	F	Sig.
Between groups	8.8	2	4.44	0.301	0.746
Within groups	132.57	9	14.73		
Total	141.45	11			

4. Conclusion

The relevance of geographic information systems and remote sensing has been explored in this study, revealing the great help these technologies can offer in monitoring LULC change and associated consequences of variations in LST conditions. This research aimed at assessing the daytime urban heat island in Onitsha has shown that loss of vegetal cover and cultivable land leads to increased LST conditions where built-up becomes a dominant land use. It also showed that such land cover conversion to built-up surfaces is intensifying the UHI effect and can affect the physiological conditions in nearby peri-urban areas through an increase in rural temperature. To achieve the SDG goal 11.6, to reduce the environmental impact of cities, it is, however, imperative that control measures be put in place to reduce the potential impact of UHI intensification when unchecked and to maintain environmental sustainability in the study area.

REFERENCES

Abuloye, A. P., Popoola K. S., Adewale, A. O., Onana V. E., and Elugoke N. O. (2015). Assessment of Daytime Surface Urban Heat Island in Onitsha, Nigeria. NMetS 2015 International Conference and 29th Annual General Meeting.

Adinna, E.N., Enete, C.I., and Okolie, T. (2019). Assessment of urban heat island and possible adaptations in Enugu urban using landsat-ETM. African Journal of Geography and Regional Planning, 6(3), 1-7

Anambra State Government (2022). A Survey of Urban Wash In Anambra State, Nigeria. Mimeographed.

Andualem T.G., Belay G. and Guadie A. (2018). Land use change detection using remote sensing technology. J. Earth Sci Clim Change, 9 (10), 1 – 6.

Ayanlade, A. (2016). Seasonality in the daytime and night-time intensity of land surface temperature in a tropical city area. Science of Total Env., 557-558, 415 – 424.

Choi Y., Myoung-Seok Suh, and Ki-Hong Park (2014). Assessment of Surface Urban Heat Islands over Three Megacities in East Asia Using Land Surface Temperature Data Retrieved from COMS. Remote Sensing, *6*, 5852-5867

Choudhury, U., Singh, S.K., Kumar, P., and Kanga, S. (2023). Assessing land use/land cover changes and urban heat island intensification: A case study of Kamrup Metropolitan District, Northeast India (2000-2032). Earth, 4 (3), 503-521. https://doi.org/10.3390/earth4030026

Enete, I.C. (2015). Urban Heat Island Research of Enugu Urban: A Review. International Journal of Physical and Human Geography Vol.3, No.2, pp.42-48,

Jumari, N.A.S.K., Ahmed A.N., Huang Y.K., Lin Ng J., Koo C.H., Chong K.L., Sherif M., and Elshafie, A. (2023). Analysis of urban heat islands with landsat satellite images and GIS in Kuala Lumpur Metropolitan City. Heliyon, 9, 1-18.

Nzoiwu, C.P., Agulue, E.I., Mbah, S. and Igboanugo, C.P. (2017) Impact of Land Use/Land Cover Change on Surface Temperature Condition of Awka Town, Nigeria. Journal of Geographic Information System, 9, 763-776. https://doi.org/10.4236/jgis.2017.96047

Nzoiwu C.P., Ozoemene M.L. and Emengini O.O. (2020). Detection of land use and land cover dynamics using geospatial techniques in Awka North Local Government Area, Anambra State. Nigerian Journal of Geography and Environment, 4 (2), 135 – 150.

Okoye, A. C., Ezenwaji, E. E., Nzoiwu, C. P. and Igboanugo, P. C (2024). An Investigation into Faecal Sludge Management in Onitsha Urban Area Nigeria. *IOSR J of Environ Sci, Toxi and Food Tech, 18, 1,* PP 34-44

Sahoo, S., Majumder, A., Swain, S., Gareema, Pateriya, B., & Al-Ansari, N. (2022). Analysis of Decadal Land Use Changes and Its Impacts on Urban Heat Island (UHI) Using Remote Sensing-Based Approach: A Smart City Perspective. *Sustainability*, *14*(19), 11892. https://doi.org/10.3390/su141911892

Yang Q., Huang X. and Li J. (2017). Assessing the relationship between surface urban heat islands and landscape patterns across climatic zones in China. Scientific Reports, 7, 9337, 1-11.

Tiwari, A.K., and Kanchan, R. (2024). Analytical study on the relationship among land surface temperature, land use/land cover, and spectral indices using geospatial techniques. *Discov Environ* 2 (1) 1-26. https://doi.org/10.1007/s44274-023-00021-1

Zargari, M., Mofidi, A., Entezar, A., and Baaghideh, M. (2024). Climatic comparison of surface urban heat island using satellite remote sensing in Tehran and suburbs. Scientific reports, 14(643), 1-23. https://doi.org/10.1038/s41598-023-50757-2

Zhang, Z., Paschalis A., Mijic A., Meili N., Manoli G., van Reeuwijk and Fatichi S. (2022). A mechanistic assessment of urban heat island intensities and drivers across climates. Urban Climate, 44, 1-18.

Zhou, B. (2017). On the assessment of surface urban heat island, size, urban form and seasonality. Institutional Repository of the University of Potsdam. http://nbn-resolving.de/urn:nbn:de:kobv:517-opus4-404383